Colloids and Surfaces A 584 (2020) 123943

Contents lists available at ScienceDirect

Colloids and Surfaces A

journal homepage: www.elsevier.com/locate/colsurfa

Spontaneous fingering between miscible fluids

Wen Song[a,b,*], Natarajan N. Ramesh[a], Anthony R. Kovscek[a]

[a] Department of Energy Resources Engineering, Stanford University, Stanford, USA
[b] Department of Petroleum and Geosystems Engineering, University of Texas at Austin, Austin, USA

GRAPHICAL ABSTRACT

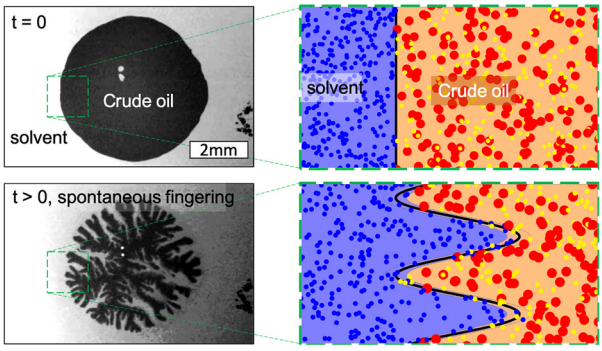

ARTICLE INFO

Keywords:
Miscible fluid interface
Diffusive mixing
Spontaneous fingering
Solvent oil recovery

ABSTRACT

Diffusion-initiated interfacial dynamics between two miscible fluids are investigated. Heptane is diffused into viscous crude oil in a microscale Hele-Shaw cell. No external pressure gradients are applied; hence, the imposed Peclet number is zero. Surprisingly, the diffusive/dispersive process is dictated by a two-stage dispersive mechanism owing to the multicomponent character of the crude oil. Stage I is distinguished by the spontaneous fractal-like fingering of heptane into the crude oil phase due to diffusive preferential light components extraction from the crude oil. Stage II is characterized by diffusive miscible fluid-pair mixing between the heptane and the heavy components in the crude oil. Preferential diffusive extraction of light components exceeds the diffusion between heptane and heavy components in stage I, thereby allowing a distinct interface to form between heptane and the crude oil. Compositional gradients induce dynamic interfacial tension gradients that lead to convection. Convection cells at the finger tips dictate local mass exchange and drive the self-similar fractal-like finger splitting. Fractal analysis of the fingering process shows increasing fractal dimensionality during the early diffusively-dominant fingering regime approaching that of diffusion-limited aggregation ($D_f \sim 1.67$), and a drastic decrease in fractal dimensionality thereafter due to small-scale convection ($D_f \sim 1.55$). We characterize the fractal finger growth and mass exchange, and calculate the local dynamic interfacial tension. We find that spontaneous fingering, i.e., the occurrence of stage I, requires gap spacing less than 15 μm in the current system and the presence of light extractable components in the crude oil.

* Corresponding author at: Department of Petroleum and Geosystems Engineering, University of Texas at Austin, Austin, USA.
E-mail address: wensong@utexas.edu (W. Song).

https://doi.org/10.1016/j.colsurfa.2019.123943
Received 1 August 2019; Received in revised form 5 September 2019; Accepted 6 September 2019
Available online 10 October 2019
0927-7757/

1. Introduction

Heavy oil, extra heavy oil, and bitumen consist of about 70% of global oil resources [1]. Recovery of this resource, however, is impaired due to its large viscosity [2] and the complexity of its transport under porous micro-confinement [3]. Thermal methods such as steam drive, cyclic steam stimulation (CSS), and steam assisted gravity drainage (SAGD) have been applied successfully to reduce the crude oil viscosity in siliciclastic formations [4,5], but require intensive energy input, often from burning other fossil fuels, and freshwater resources. The resulting thermal enhanced oil recovery process is therefore disadvantaged environmentally.

Promisingly, solvent-assisted extraction provides a means to enhance oil recovery, reduce materials and energy input, and limit the environmental impacts that are typically associated with thermal viscosity-reduction processes (c.f., Boone et al. [6]). Specifically, light miscible hydrocarbon solvents such as propane, pentane, and heptane improve crude oil recovery by reducing the viscosity of the crude oil through diffusive mixing [7] to provide an economic and environmentally benign path to recover viscous crude oils [8,9]. Complex crude-oil compositions and unresolved solvent-crude oil mixing dynamics at the microscopic pore-scale, however, lead to significant uncertainties in the macroscopic reservoir-scale behavior of the recovery process. Specifically, mixing dynamics of solvent into the crude oil, swelling of crude oil due to solvent dissolution [10], and potential formation damage due to solvent particle precipitation [11] must be resolved. These are all pore- and interface-level dynamics that must be described at the microscale.

Investigation of fundamental interfacial behavior of reservoir fluids at the microscale are enabled by recent advances in microfluidic devices. Advantageously, microfluidic platforms allow direct insight into the diffusive/ dispersive dynamics that dictate solvent-enhanced oil recovery in porous media at the relevant length (~μm) and time scales (~ms) of subsurface flows [12–18]. Fundamental investigations on phase behavior, interfacial dynamics, and solvent-crude oil mixing are enabled by simple microfluidic devices [12,15,16,19,20]. One simple microfluidic geometry used to probe immiscible fluid-pair dynamics is the Hele-Shaw configuration [21–25] where the dynamics of fluids between two parallel plates are delineated directly. Experimental and theoretical developments in the literature show results for low viscosity fluids injected into resident high viscosity fluids within Hele-Shaw cells. The two parallel plates comprising the Hele-Shaw configuration are maintained at a fixed distance (~mm–cm) to mimic the permeability of porous rock material. The Hele-Shaw configuration has formed the basis of analytical solutions to the interfacial instabilities observed when a fluid with low viscosity (e.g., an injectant) displaces one with higher viscosity (e.g., the crude oil) [21,26–28]. The Saffman-Taylor solution, for instance, describes the interfacial instabilities that arise due to the injection of an immiscible low viscosity fluid into a high viscosity fluid in a Hele-Shaw configuration.

More recent studies on partially miscible fluid-pairs have been motivated by a number of practical applications, including CO_2 storage and enhanced oil recovery [7,8,27–33]. Notably, experiments conducted using fluid-pairs at the low interfacial tension condition, typically single-component fluids such as glycerol and water, show surprising dynamics between the initially distinct fluid phases, such as regularity in interfacial instabilities and the existence of ramified fingering during injection [30,32]. Such high capillary number (Ca = viscous forces/surface tension) and low Peclet number (Pe = imposed advection rate/diffusion rate) systems result in complex interfacial instabilities that arise due to competing driving forces. Furthermore, recent modeling of miscible fluid-pair mixing due to externally-driven flow- and buoyancy-forcing shows complex fingering dynamics [34,35], and uses the idea of Korteweg stresses to describe the complex mixing behavior [36–39]. Specifically, Korteweg stresses are transient, tangential stresses introduced to account for diffusive mass exchange that is not present in classical immiscible fluid-pair descriptions of mass and momentum conservation. In keeping with conditions that represent subsurface processes such as oil recovery or carbon sequestration, further delineation of the dynamics at fully miscible, low flow, and complex fluid composition conditions are required.

Insofar as the literature has delineated the mechanisms underlying interfacial dynamics between simple miscible fluids, diffusion-initiated mixing between multicomponent, fully miscible fluids at the low flow, micro-confined scale has scarcely been explored experimentally. In this work, we examine oil recovery mechanisms due to solvent-crude oil dispersion at microscopic length scales due to diffusively-driven fluid mixing. As outlined above, existing literature examines the interfacial dynamics between immiscible and miscible fluids due to injection of a low viscosity fluid into a high viscosity fluid. As an analog to far-from-well conditions and cyclic single-well processes, we probe the interfacial dynamics between miscible fluids in the absence of external pressure gradients and imposed flows.

2. Experimental methods

Microscale solvent-crude oil mixing dynamics underlying solvent-enhanced oil recovery were visualized in a glass micro-Hele-Shaw cell. Heptane (Heptane, H350-4, Fisher-Scientific) was chosen as the solvent phase due to its miscibility with crude oils. Viscosity of heptane at the experimental conditions is 0.42 cP. The properties of the crude oil are listed in Table 1. Specifically, the crude oil chosen has a viscosity of 87.7 cP. The viscosity ratio of this fluid-pair is hence $\eta_{crude\ oil}/\eta_{solvent} = 209$. Fig. 2 shows the complex compositional character of the crude oil.

Interfacial dynamics between the solvent and crude oil were investigated in a microscale Hele-Shaw-type apparatus (Fig. 1). A single crude-oil droplet was sandwiched between two horizontal glass plates to minimize gravitational mixing. Gap spacing between the glass plates was set to 5, 15, and 30 μm to investigate the effect of length scale. Stainless steel shim stock was used to maintain the gap spacing. Solvent droplets dispensed near the edges of the cover plate entered the flat cell via capillarity. No external pressure gradients or injections were applied to drive the flow. All experiments were conducted at ambient temperatures and pressures and the system boundary was held at constant pressure. Boundaries were also submerged in heptane. A microscope (Leica Z16 APO Macroscope) and camera (Leica DFC 450) were used to capture the dynamics directly. The dynamics were recorded at 25 frames per second.

3. Results

3.1. Spontaneous two-stage mixing

Diffusive mixing between the miscible crude oil and solvent pair, in the absence of external pressure gradients or flow impositions, resulted in a surprising two-stage mixing phenomenon (Fig. 3). Specifically, for a Hele-Shaw cell with a gap spacing $b = 5$ μm, heptane and crude oil mixed in two markedly distinct stages: spontaneous formation of fractal-like fingers at short times (i.e., Stage I, Fig. 3, $t = 0$ s to $t = 24$ s) and slow diffusive mixing thereafter (i.e., Stage II, Fig. 3, $t = 24$ s to $t = 91$ s). Anomalously, in the absence of external pressure gradients or

Table 1
Crude oil characterization [40].

Crude oil properties	Value
Acid number (mg g^{-1})	0.83
Base number (mg g^{-1})	2.87
Viscosity at 22 °C (cP)	87.7
Asphaltene content (wt %)	6.2
Specific gravity	0.918

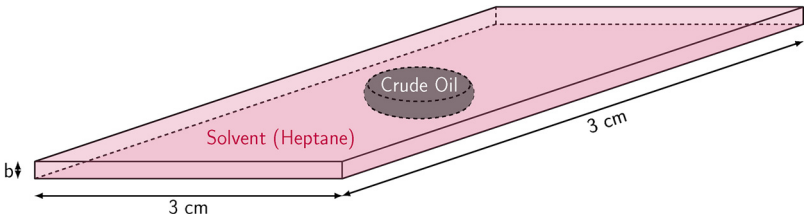

Fig. 1. Microscale Hele-Shaw cell with gap spacing, b, of 5, 15, and 30 μm. A single crude oil droplet is encased between the top and bottom plates and heptane solvent is introduced. Heptane and crude oil are miscible and the system boundaries are held at constant pressure and immersed in heptane. No external pressure gradient or flow is imposed.

flow, the mixing timescale for a crude-oil droplet with a radius of ~2.5 mm was on the order of ~1 min. In contrast, purely diffusion driven interaction timescales are expected to be ~1 h for a typical crude oil-heptane diffusivity of $D \sim 1.5 \times 10^{-5}\,\mathrm{cm}^2/\mathrm{s}$ [41]. The observed spontaneous fractal-like fingering was therefore not driven by diffusion alone.

3.2. Dependence on crude oil composition.

Robustness of this spontaneous fingering phenomenon was corroborated using a series of crude oils with different compositions that resulted in a range of volatilities and viscosities. The degree of spontaneous fingering was found to be related to the composition of the crude oil. Specifically, volatile crude oils containing both small, mobile molecules and large, relatively immobile molecules experienced the spontaneous fingering phenomenon repeatably (Fig. 3). With decreasing volatility and increasing viscosity (i.e., crude oils with fewer small, mobile components), fewer stable fingers were propagated.

At the extreme, crude oils with only large immobile molecules showed no spontaneous fingering. The same result was observed for devolatized crude oils where light components had been expelled. Mixing between nonvolatile crude oil and solvent was consistent with bulk-scale diffusion (Fig. 4). The degree of spontaneous fingering, therefore, increases somewhat with the volatility of the crude oil. While it is difficult to ensure that these results will apply to all petroleum reservoirs owing to the heterogeneities in crude oil composition, the experimental results show that spontaneous fingering occurs for moderately volatile and viscous crude oils that consist of both light and heavy components.

3.3. Dependence on gap spacing

The anomalous spontaneous fingers are unique to microconfinement and are not observed at the bulk-scale. Scale-dependence of the phenomenon is therefore suggested.

The degree of spontaneous fingering between crude oil and solvent pairs were investigated with respect to the gap spacing between the parallel Hele-Shaw plates. Mixing dynamics were characterized under gap spacings of b = 5, 15, and 30 μm. For the crude oil composition described in Table 1, a critical gap spacing of $b_{crit} \sim 15$ μm was found as the cut-off length, i.e., minimum pore-size, at which the specific fluid pair fingers spontaneously (Fig. 5, b = 15 μm). That is, fingering occurred spontaneously for gap spacings below the cut-off length scale, b < 15 μm (Fig. 5, b = 5 μm), and was absent for gap spacings above the cut-off length-scale, b > 15 μm (Fig. 5, b = 30 μm). Experiments with different crude oils show that the cut-off gap spacing is dependent upon the composition of the crude oil. For fixed microscale gap spacings, impressively, the fingers were spaced evenly. A gap spacing of b = 5 μm, for example, resulted in critical unstable wavelengths, that is, the instability wavelengths at which fingers propagate [21], of $\lambda_c \sim 272\,\mu\mathrm{m} \pm 69\,\mu\mathrm{m}$ (Figs. 6 and 5). The critical wavelength for a b = 15 μm gap spacing was $\lambda_c \sim 820\,\mu\mathrm{m}$ (Fig. 5), showing diminishing instability with scale. In the subsurface, these results suggest that tighter formations, i.e., reservoirs with small pore-sizes, are most susceptible to the enhanced mixing due to spontaneous fingering.

4. Discussion

Under no external pressure gradients, a surprising two-stage diffusive process was observed wherein solvent appears to finger spontaneously into a complex crude oil containing both heavy and light fractions. The same miscible fluid-pair mixes diffusively under bulk conditions, and measurements of bulk-scale interfacial tension are not possible due to the lack of a distinct interface. It is therefore surprising, then, that under microconfinement, the two fluids form distinct phases and that mixing is enhanced by the formation of spontaneous fingers.

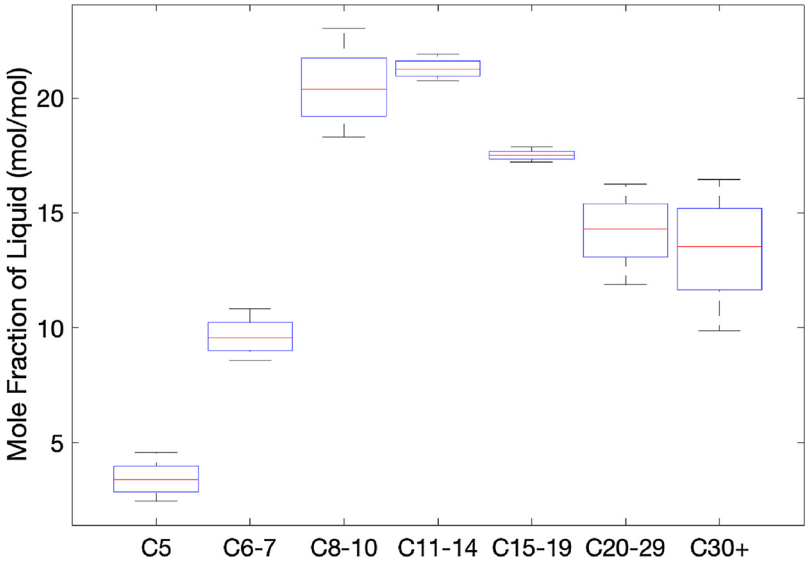

Fig. 2. Composition of the crude oil by carbon number (C). This crude oil is comprised of both lighter (C5–10) and heavier (C11 +) components. Light components are mobile and capable of relatively rapid diffusion, whereas heavy components are less so.

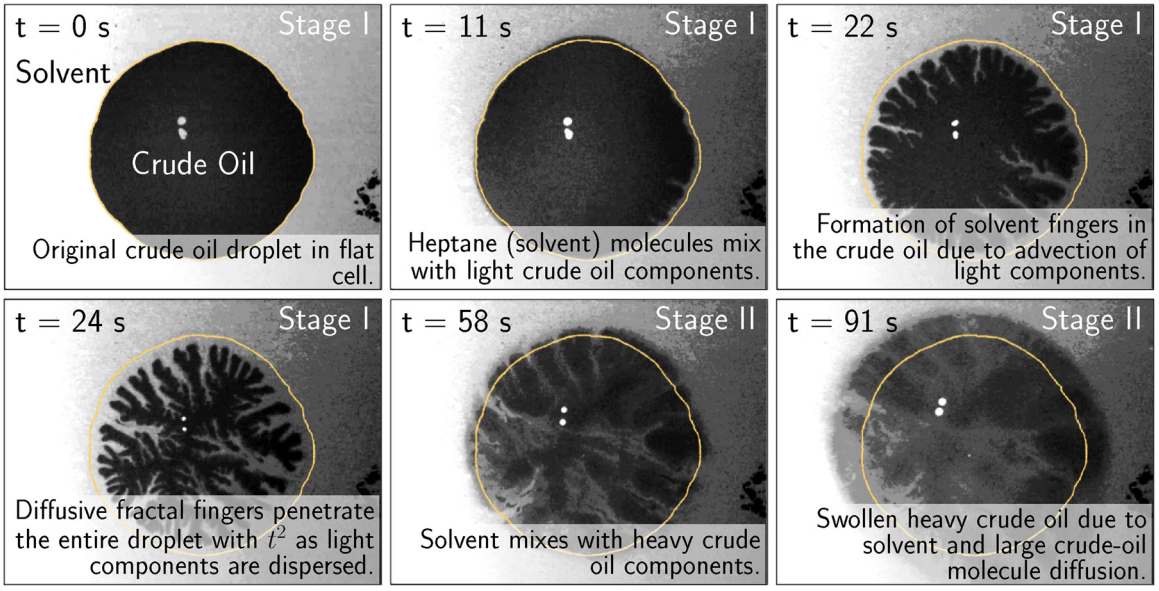

Fig. 3. Hele-Shaw cell experiment of mixing dynamics between heptane and the crude oil. The orange circle denotes the original drop shape. Stage I ($t = 0$ s to $t = 24$ s) is characterized by rapid mixing that is dictated by fractal-like fingers that develop spontaneously into the crude-oil droplet. This stage is fast and on the order of 10's of seconds. Stage II ($t > 24$ s) is characterized by slower (on the order of minutes) mixing between the solvent and the crude oil phases that is described by bulk-phase diffusion. (For interpretation of the references to color in this figure legend, the reader is referred to the web version of this article.)

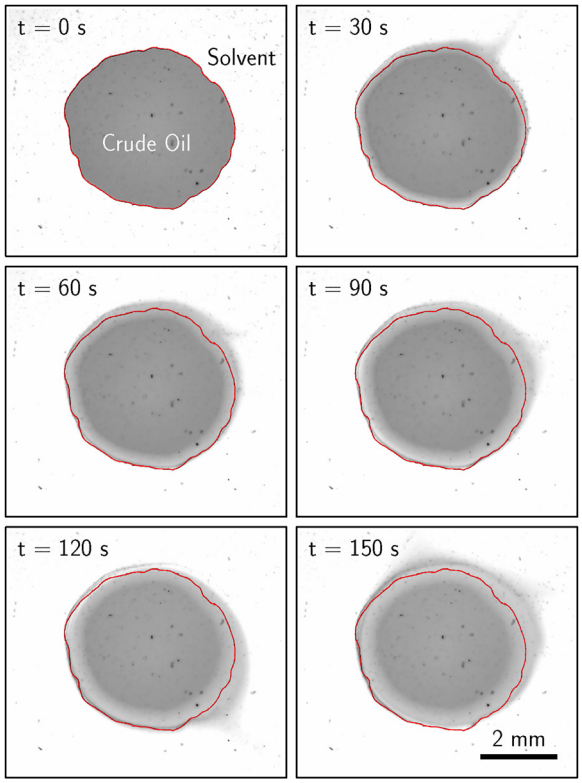

Fig. 4. Perturbations to the interface were not observed for non-volatile crude oil and solvent pairs where the light, volatile components in the crude oil were liberated in advance of the experiment.

Importantly, the anomalous spontaneous fingering was observed only for crude-oil samples containing both heavy and light components (Fig. 3) and was not observed in oil samples with only heavy components (Fig. 4). The reliance of the spontaneous fingering phenomenon on crude oil composition (Figs. 3 and 4) suggests that the two-stage diffusive process may be attributed to the multicomponent character of the crude oil.

4.1. Two-stage mixing due to multicomponent character of crude oil

In volatile crude oil, small, lighter components are mobile (diffusivity $D \sim 1/d$, where d is the molecular diameter) and are susceptible to diffusion [42]. Heavy, branched components, on the other hand, are less mobile in comparison and their self-affinity retains the heavy components in the original crude oil phase. Similarly, lighter components enable the diffusion of other species, such as the solvent heptane, to diffusive easily, whereas heavier components retard the diffusion of such solvents. As a result, when in contact with a miscible solvent such as heptane, differential rates of diffusion arise due to molecular size and mobility.

In the case of the dynamics shown in Fig. 3, spontaneous fractal-like fingering of stage I (Fig. 3, $t = 0$ to 24 s) is attributed to the mutual diffusion of light crude-oil components into the solvent phase and heptane molecules into the crude-oil phase. We observe preferential diffusive extraction of light components out of the crude-oil phase and the diffusion of heptane into the crude-oil phase over time. Light components extraction is evidenced through reductions in droplet size compared to the initial conditions (Fig. 3, $t = 24$ s vs. $t = 0$ s), and is consistent with the zero-net-flux condition for multicomponent diffusion [43]. Contact between crude oil and the solvent creates a sharp concentration gradient that drives rapid migration of (i) light component molecules out of the crude-oil phase and into the solvent phase, and (ii) heptane molecules out of the solvent phase and into the crude-oil phase. Immobile heavy components, however, are left behind and concentrated in the crude-oil phase. This results in the observed preferential diffusive extraction and fingering.

The fractal-like fingering process continues until light, mobile components are extracted preferentially by diffusion. Full extraction of the light components marks the conclusion of spontaneous fingering in stage I and the onset of slow diffusion in stage II. Specifically, heavy crude-oil molecules diffuse into the solvent phase (Fig. 3, $t = 24$ to 91 s) and heptane molecules diffuse into the crude-oil phase, causing the crude oil phase to swell beyond its initial size (Fig. 3, $t = 58$ to 91 s). Diffusive mixing during stage II blurred out the fractal-like fingers formed during light-components extraction in stage I.

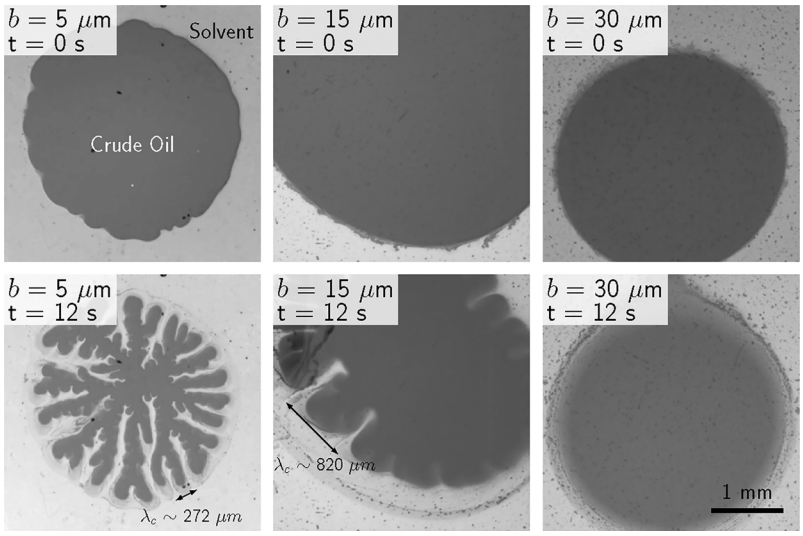

Fig. 5. Occurrence of spontaneous fingering with gap spacing. Critical wavelengths λ_c are observed to scale with the gap spacing, b. The cut-off length-scale in the present crude oil – heptane system is a gap spacing of $b \sim 15\,\mu m$. Larger gap spacings, i.e., larger pore spaces, do not benefit from the enhanced mixing of spontaneous fingering.

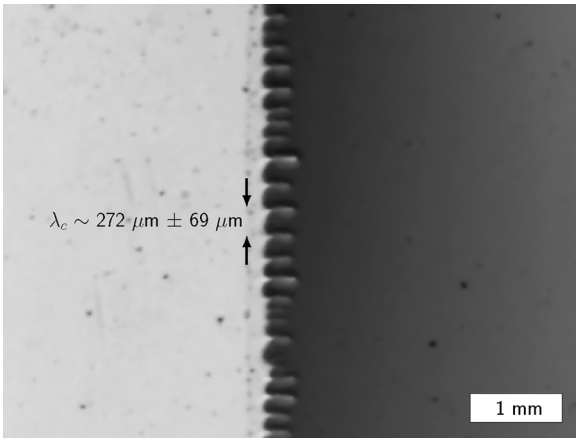

Fig. 6. Most unstable wavelength. The system consistently exhibits fingering at the most unstable wavelength of $\lambda_c \sim 272\,\mu m \pm 69\,\mu m$ for a gap spacing of 5 μm.

4.2. *Interface characteristics: self-similarity in finger splitting due to recursive diffusive-hydrodynamic perturbations*

The spontaneous fingers that propagated into the crude oil droplet exhibit self-similarity. Characterization of fingering fractal dimension based on interfacial contact area (Fig. 7) and of volumetric evolution (Fig. 8) show that the fractal dimensionality of the fingers range from $D_f = 1.55$ to 1.67 for a gap spacing of 5 μm over time. Fractal dimensions were obtained through characterization of the interface delineated by the invading fingers using box counting. Specifically, the FracLac plugin from ImageJ was used to quantify the fractal dimensions. Changes in the fractal dimensions of the mixing phenomenon delineates three regimes: (i) a diffusively-dominant regime (Fig. 8b,c green) where fractal dimensionality increases and droplet size decreases linearly, (ii) a hydrodynamically-dominant regime (Fig. 8, $t = 7.84$ to 12.08 s, b,c yellow) where both fractal dimensionality and droplet sizes decrease rapidly, and (iii) another diffusively-dominant regime (Fig. 8b,c red) where fractal dimensions increase and droplet sizes decrease rapidly.

Regime I, in which fractal dimensions increase and droplet volumes

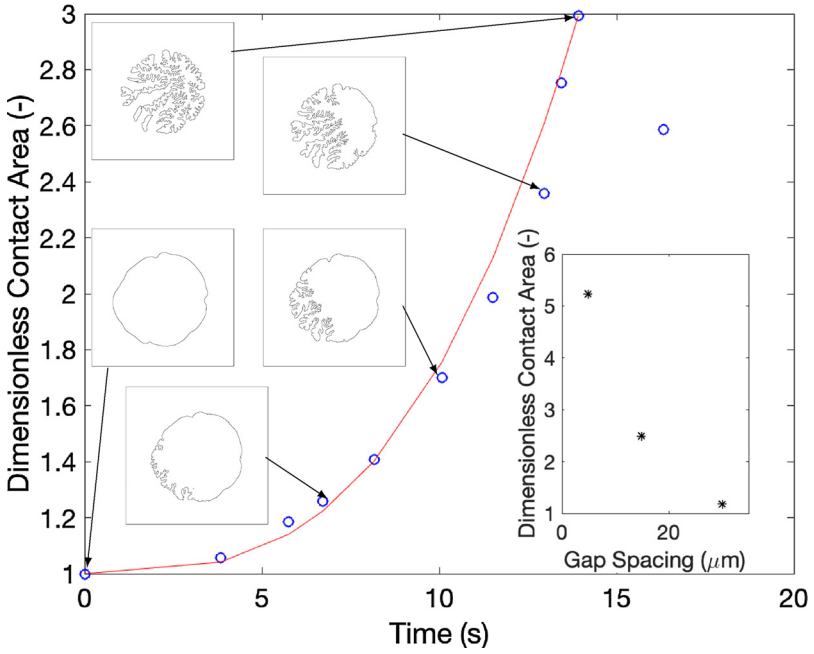

Fig. 7. Time-evolution of interfacial contact area between the crude oil and solvent over time. Contact area, delineated by the length of the interface, is normalized based on the initial interface (blue). The dimensionless contact area increases faster than that of classical diffusion as approximately the cubic of time (red) due to dispersion driven by fluid mixing. Dimensionless contact area at a fixed time 10 s is shown as a function of gap spacing in the inset to demonstrate the increasing importance of the fingering mechanism on effective mixing rates at small scales. (For interpretation of the references to color in this figure legend, the reader is referred to the web version of this article.)

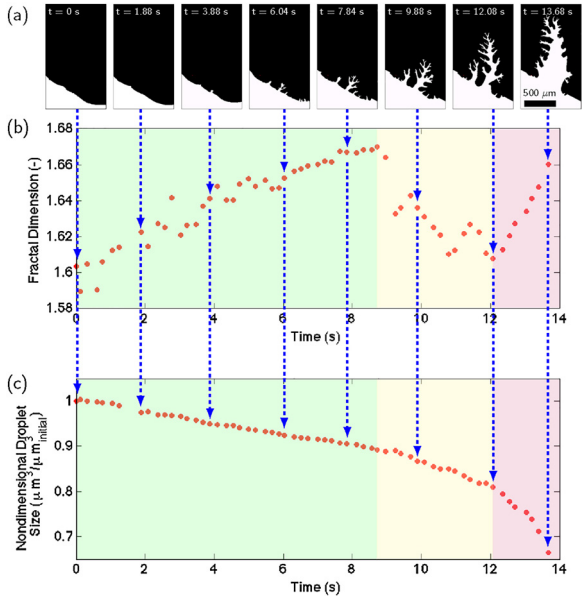

Fig. 8. Time-evolution of interface fractal dimension showing the fingering process between one-dimensional advection and diffusion-limited aggregation for the crude oil with both heavy and light components under 5 μm gap spacing confinement [45]. Absence of an imposed flow on this system results in initial diffusively-dominant mass exchange between the solvent and light components in the crude oil (t = 0 s to t = 8.72 s). The resulting interfacial destabilization process is fractal-like in that each perturbed interface is perturbed recursively. Diffusively-driven interfacial perturbation from a flat interface ($D_{f,flat}$ = 1) towards a diffusion-limited aggregation condition ($D_{f,DLA}$ = 1.68 ± 0.04) is characterized by a growth in fractal dimensionality from D_f = 1.55 to D_f = 1.67. Diffusion-driven growth is sustained until hydrodynamic forces dominate (t = 8.72 s to t = 10.96 s), resulting in enhanced mass exchange between the crude oil and the solvent. Reduced diffusive miscible fluid pair mixing in relation to hydrodynamics hinder the interfacial instability, resulting in a more one-dimensional finger and the reduced fractal dimensions (D_f = 1.67 to 1.58) of the local interface. Mass exchange at late times (t > 10.96 s) is limited due to excess solvent and scarce light components available for extraction from the crude oil. This enables a return to the diffusively-dominant regime where interfacial instabilities develop and correspond to the increase in the local fractal dimension from D_f = 1.58 to 1.66. (For interpretation of the references to color in the text, the reader is referred to the web version of this article.)

decrease linearly, is dictated by the mutual exchange of mass between the solvent and light components in the crude oil. The diffusively-driven fingering results in compositional gradients along the crude oil-solvent interface, and hence gradients in density, viscosity, and dynamic interfacial tension. In our system, preferential diffusive light components extraction (i.e., heavy components concentration) induce a gradient in dynamic interfacial tension that destabilizes the interface to drive the fingering process. During the early diffusion-driven interfacial perturbation regime (Fig. 8, t = 0 to 1.84 s, green), fractal dimensionality increases from a flat interface towards D_f = 1.67 due to finger splitting that approaches diffusion-limited aggregation (DLA, $D_{f,DLA}$ = 1.68 ± 0.04) [44,45]. Indeed, the pattern formed during the spontaneous fingering process is reminiscent of the DLA model of Witten and Sander [46,47]. Specifically, the interfaces are destabilized in a recursive manner, similar to the sticking of monomers to a cluster [44,48,49]. One can view the initial interfacial instabilities (Fig. 12b) as the "monomers", and its growth and recursive destabilization as the "sticking of additional monomers". Interfacial destabilization due to diffusion-driven mass exchange, hence, is a fractal-like process in that each perturbed interface is perturbed recursively, resulting in an approximately linear growth in its fractal dimension.

Regime II, in which both fractal dimensions and droplet volumes decrease, marks a hydrodynamically-dominant regime (Fig. 8, t = 7.84 to 12.08 s, b,c yellow). The interfacial fluid property gradients developed in regime I result in a Marangoni-like instability that enables convective dynamics to dominate in regime II. Dominant Marangoni-driven convection in place of diffusion-driven mixing results in enhanced mass exchange between the crude oil and solvent phases. The significance of the Marangoni effect in this case is measured by the Marangoni number

$$\mathrm{Ma} = \frac{\delta\sigma}{\delta C}\frac{L\Delta C}{\eta D} \tag{1}$$

where $\delta\sigma/\delta C$ is the change in interfacial tension with concentration and ΔC is the total change in concentration across the characteristic length L for a fluid with viscosity η and diffusivity D. For the present fluid system, taking the characteristic length of the droplet radius $L \sim 1$ mm and a maximum interfacial tension differential of $\delta\sigma \sim 40$ mN/m (see Section 4.3), we arrive at a Marangoni number of $Ma \sim 3 \times 10^5$, a regime in which significant Marangoni convective cells are expected.

Convective cells born of dynamic interfacial stresses expedite mixing in the heptane phase; convection enables removal of the extracted light components from the interface and accelerates the rate at which light components are extracted subsequently. Development of new interfacial perturbations, however, is hindered in this stage, resulting in more rectilinear, i.e., decreasing fractal dimensionality (D_f from 1.67 to 1.58), fingering. Growth rates of finger areas and finger lengths deviate from purely-diffusion-driven mass exchange (Figs. 10 and 11). Characterization of the rate at which the light components are extracted shows that the volume of light components extracted from the

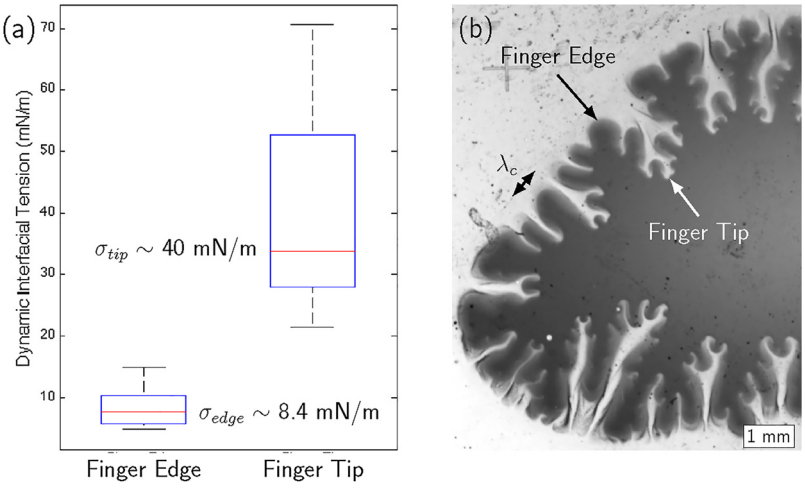

Fig. 9. Dynamic interfacial tension between the crude oil and the heptane. Interfacial tension is estimated using experimental measurements of the characteristic wavelength, λ_c, the gap separation, b = 5 μm, and the interfacial velocity, V. The maximum and minimum induced interfacial velocities are measured at the finger tip and the finger edge, respectively, to calculate the maximum and minimum dynamic interfacial tension. The calculations show a clear gradient in the dynamic interfacial tension.

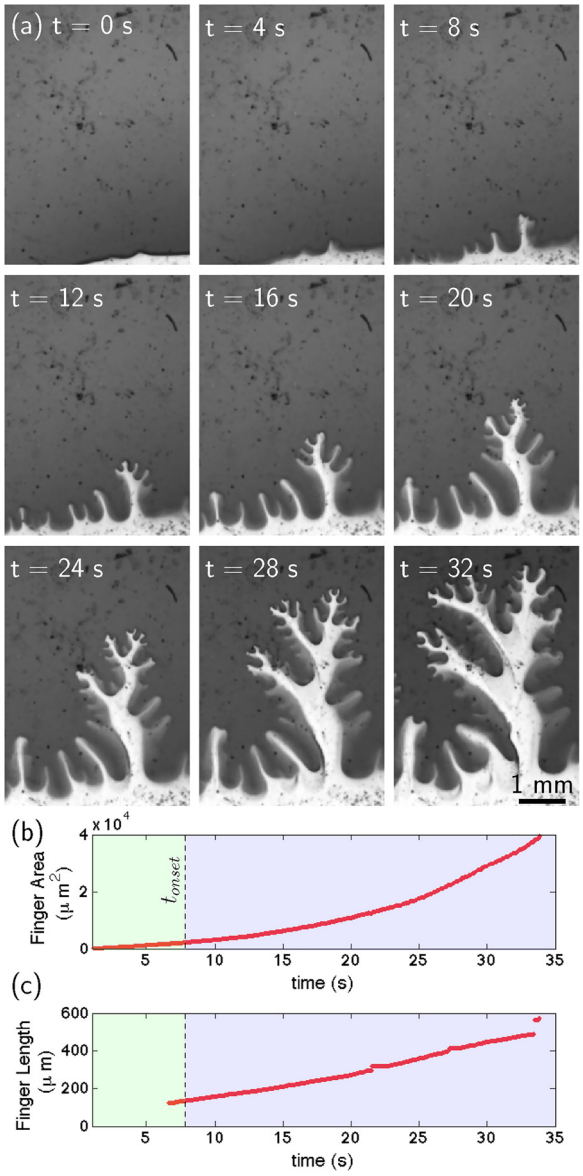

Fig. 10. Velocity of fractal-like finger propagation and preferential diffusive light components extraction for a gap spacing of $b = 5$ μm. (a) Fingering evolution at different times. Self-similar fractal-like fingers propagate at a constant velocity into the crude-oil phase. Finger-splitting at the tip of the finger occurs at the same characteristic wavelengths ($t = 8$ to 32 s), demonstrating the self-similar nature of the fractal-like fingers. The finger tip wavelengths, however, are shorter than the finger edge wavelengths, suggesting that convection cells generated by gradients in dynamic interfacial tension dictate splitting of the self-similar structures. (b) Finger area, a proxy for light components extraction from the crude-oil phase into the solvent phase, deviates from purely-diffusion-driven mass transport upon the onset of finger splitting. (c) Velocity of dominant finger propagation into the crude-oil phase scales with the square of time (Length$^{1/2} \sim t$) as dictated by mixing in the convection cells. (For interpretation of the references to color in the text, the reader is referred to the web version of this article.)

crude oil scales initially with the ~1.5 power of time (Figs. 10(b, green) and 11a), consistent with dispersive transport normal to the convective flow direction (Fig. 10, $t = 0$ to 8 s). After the onset of finger splitting (Fig. 10, $t = 8$ s), the power transitions from 1.5 to about 2 between normalized times of 2 and 3 (Fig. 11(b)). As normalized time becomes greater than about 3 (24 s), the power increases again due to fractal-growth and finite size effects of the heptane fingers growing into the crude-oil phase. The average power following the onset of finger splitting is 2. The finger length (Fig. 10c) penetrates with the square of time (i.e., Length $\sim t^2$).

Regime III returns to a diffusively-dominant regime (Fig. 8b,c red) where fractal dimensions increase from $D_f = 1.58$ to 1.67 and droplet sizes decrease rapidly due to limited mass exchange in the presence of excess solvent and scarce availability of light components available for extraction from the crude oil.

4.3. Existence of distinct interfaces

Existence of distinct finger interfaces suggest that the local advection rates induced by spontaneous fingering far exceed the local diffusive rates at the finger scale [26,27,30]. In pressure-driven Saffman-Taylor fingering, instabilities are driven by the most unstable wavelength, λ_c, given by:

$$\lambda_c = \pi b \sqrt{\frac{\sigma}{\Delta\eta V}} \tag{2}$$

where b is the gap spacing between the glass plates, σ is the interfacial tension, $\Delta\eta$ is the difference in viscosity between the crude oil and solvent phases, and V is the interfacial velocity imposed by an external pressure gradient [21,30,50]. The present system, in contrast, is without an imposed velocity. The rate of interface retraction, i.e., the induced velocity due to heptane and light components diffusion, can be viewed as an analog of the imposed interfacial velocity in the Saffman-Taylor instability. Characterization of the growth dynamics shows that the unstable wavelength in the present system is $\lambda_c \sim 272\ \mu m \pm 69\ \mu m$ for a gap spacing of 5 μm (Fig. 6). In this system, the viscosity difference is $\Delta\eta = \eta_{Crude\ Oil} - \eta_{Heptane} = 87.3$ cP. Maximum and minimum induced interfacial velocities are delineated by measuring the induced velocities at the finger tips and finger edges, respectively (Fig. 9a). Using the characteristic wavelength relation developed by Saffman and Taylor, the corresponding maximum and minimum dynamic interfacial tensions are calculated (Fig. 9a). Importantly, we calculate an effective finger-tip dynamic interfacial tension of $\sigma_{tip} \sim 40$ mN/m and an effective finger edge dynamic interfacial tension of $\sigma_{edge} \sim 8.4$ mN/m by assuming quasi-immiscible conditions (Eq. (1)). Apparently, a spatial gradient in the dynamic interfacial tension is established across the finger as a result of light components flux across the solvent-crude oil interface. In other words, rapid mass exchange of heptane and light components between the solvent and crude-oil phases create chemical potential gradients in the crude oil that lead to gradients in dynamic interfacial tension.

Critical wavelengths for fingering instability, measured experimentally, scale with gap spacing (Fig. 5 λ_c ($b = 5\mu m$) ~272μm, λ_c ($b = 15\ \mu m$) ~820 μm). This is consistent with predictions using the Saffman-Taylor result, using an effective finger tip dynamic interfacial tension of 40 mN/m (Fig. 9), as a proxy (Table 2).

4.4. Spontaneous fingering: a mechanistic and quantitative depiction

Mutual mass exchange between the miscible fluid pair (crude oil and solvent) underlies the spontaneous fingering observed at early times. A mechanistic description of the dynamics is arrived at using time scaling. In a simplified depiction of the fluid-pair system (Fig. 12), the solvent phase is initially composed of single component heptane molecules that are small and mobile (i.e., diffusive); the crude oil phase is comprised of small, light components that are mobile (i.e., diffusive) and large, heavy components that are relatively immobile (i.e., less diffusive).

Initial molecular configurations (t_0, Fig. 12a) are such that heptane molecules (small blue circles) are confined to the solvent phase (blue) and crude oil molecules (small yellow and large red circles) are confined to the crude oil phase (orange). The initial compositional distribution leads to sharp concentration gradients, and, thus, a large

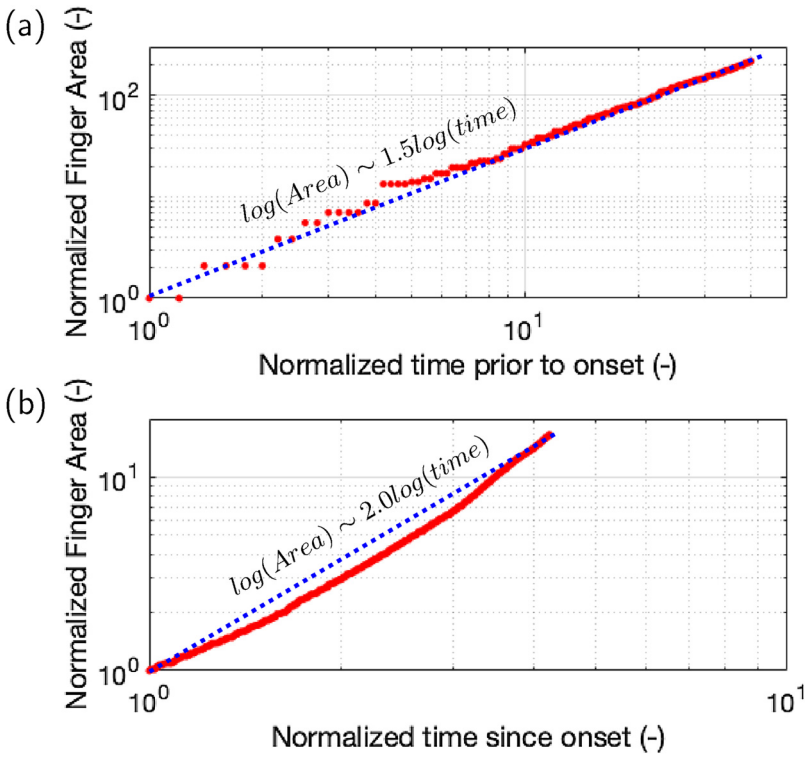

Fig. 11. Deviation of fingering rates from purely-diffusion-driven mass exchange of crude oil with both heavy and light components under 5 μm gap spacing. Finger areas are normalized to the initial (a) and onset finger areas (b), and elapsed times in each regime are normalized with initial (a) and onset time (b). Finger area scales with time to the 1.5 (a) and 2.0 (b) power prior to and following the onset of finger splitting at $t = 8$ s, respectively. (a) Early time fingering scales in accordance with dispersion and convection (Area $\sim t^{1.5}$). (b) Onset of finger splitting at $t = 8$ s transitions finger area scaling in accordance to Area $\sim t^{2.0}$.

Table 2
Critical wavelengths at varying gap spacings from experimental measurements and theoretical prediction using the Saffman-Taylor result as a proxy.

Time (s)	Gap spacing (μm)	Velocity (mm/s)	$\lambda_{c,theory}$ (μm)	$\lambda_{c,exp}$ (μm)
12	5	1.6	269	272
12	15	1.5	830	820
12	30	0.09	6700 $> d_{droplet}$	–

diffusive driving force that enables mixing in the absence of external driving forces.

Upon contact (t_{0^+}, Fig. 12b), miscibility between heptane and crude oil, in combination with the steep concentration gradient across the interface, forces mutual diffusion of heptane molecules into the crude oil phase and smaller crude-oil molecules into the solvent phase. The diffusion-driven interfacial perturbations correspond to the early-time approach towards DLA (Fig. 8a, fractal dimension $D_f \rightarrow 1.67$, and Fig. 8b,c, shaded green).

The small gap-spacing requirement is explained here due to its effect on dynamic interfacial tension and capillarity that are length-scale dependent. Specifically, small length-scale scenarios enable large interfacial curvature, and thus, significant pressure differential across the dynamic interface. Recall that the initial rate of diffusion scales with the differential of chemical species partial pressure across the two fluid phases. At small gap spacings, diffusivity of small, mobile heptane and light crude-oil molecules enable rapid mass exchange between the two initial phases. While we have explored the upper limit of pore sizes, we have not explored the lower limit for this spontaneous fingering phenomenon and leave that open for future studies. We speculate that the dynamics observed here may apply to shale systems, however other mechanisms such as capillary condensation that may be important are not captured here.

Large, viscous heavy crude-oil molecules, on the other hand, experience little mass diffusion within the solvent phase. Heavy components are viscous and so have lesser diffusivity, as diffusivity, D, correlates with viscosity, μ, as $D \sim \mu^{\epsilon}$, and the exponent ϵ is related to the molar volume, V, of the species as $\epsilon = 10.2/V - 0.791$ [51]. The intermolecular attraction between the large, immobile molecules retains the molecules in its original phase and thus the observed dark, crude oil phase. Different diffusion rates of the large and small crude-oil molecules result in differential local fluid compositions and thus gradients in local dynamic interfacial tension.

Gradients in interfacial tension resulting from variations in interfacial composition, lead to hydrodynamic perturbations to the flow ($t_{stage\ I}$, Fig. 12(c)) because interfacial fluid flows towards interface area with greater tension. With respect to fractal dimensionality, the convection dominance in this regime adds to the linearity of flow, resulting in a decreased fractal dimensionality towards one-dimensional advection and away from DLA (Fig. 8a, $D_f \rightarrow 1.55$, and Fig. 8b,c, shaded yellow). Marangoni-like convection enhances subsequent extension of the local diffusively-driven perturbations. Importantly, the composition-driven hydrodynamics here enable finger propagation at wavelengths corresponding to the local critical wavelength, λ_c. Further diffusion normal to the newly generated finger interface perturb the local interface as in Fig. 12b. Ramified fingers at early times are attributed to the recursive perturbations to the growing local interface.

Recursive diffusive-hydrodynamic mass exchange is self-sustained prior to equilibrium between the solvent and crude-oil phases ($t_{stage\ II}$, Fig. 12(d)). Micro-confinement results in crude-oil droplets of finite volume, similar to crude-oil droplets residing in petroleum reservoirs, and limits the fingering process to a finite lifetime. Specifically, as the heptane and light crude-oil molecules in the interface between the solvent and crude-oil phases approach equilibrium, the compositionally-driven diffusive-hydrodynamic transport underlying the fingering process is eliminated and stage II begins. Stage II is marked by the slow mixing of large, immobile molecules in the crude oil phase with components in the solvent phase that results in a classic diffusive mixing zone otherwise observed in bulk dimensions. The return to a diffusively-dominant regime restores the fractal dimensionality towards DLA (Fig. 8a, $D_f \rightarrow 1.67$, and Figs. 8b,c, shaded red).

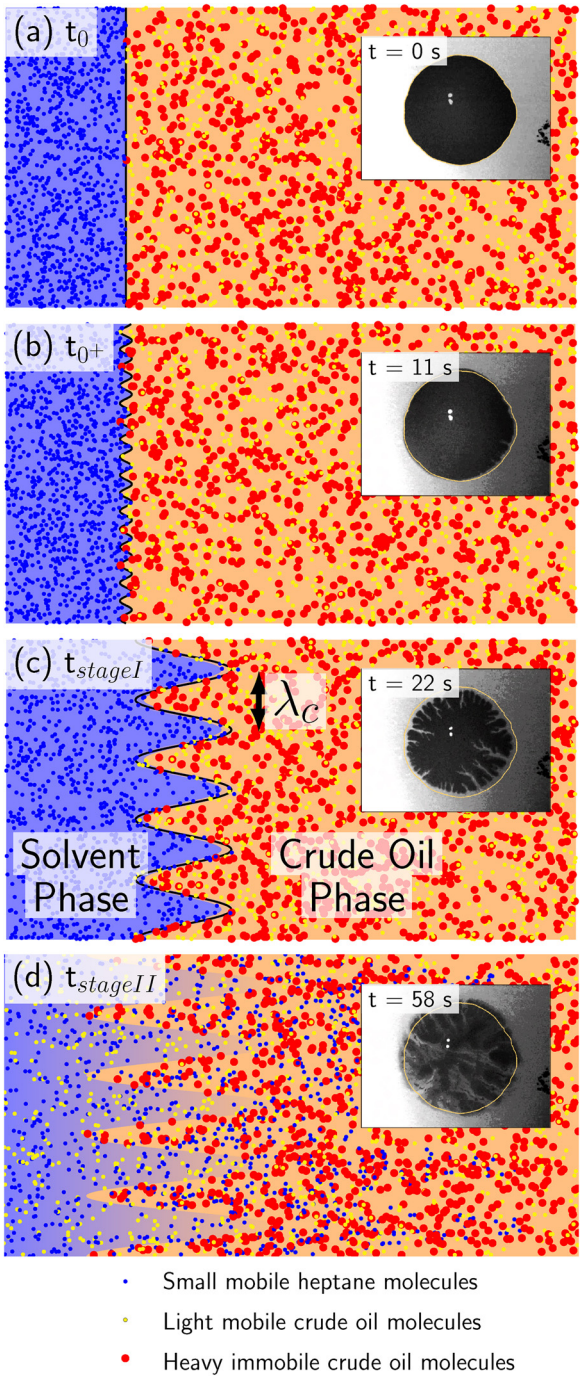

Fig. 12. Mechanistic depiction of spontaneous fractal-like fingering between crude oil and heptane corresponding to experimental results of Fig. 3 where a crude oil with heavy and light components is confined to a 5 μm gap spacing. (a) Initial fluid distributions ($t = 0$) with small mobile heptane molecules (blue) in the solvent phase (blue) and light, mobile (yellow) and heavy, relatively immobile (red) crude oil molecules in the crude oil phase (orange). (b) Mutual diffusion of heptane molecules and light, mobile crude oil molecules drive interfacial perturbations at very early times (t_{0^+}) that initiate interfacial stability. (c) Instabilities corresponding to the most unstable wavelength, λ_c, drive pressure and dynamic interfacial tension gradients during stage I ($t_{stage\ I}$). Local gradients in composition drive mass exchange across the interface and result in gradients in the local dynamic interfacial tension. The dynamic interfacial stresses drive mass exchange hydrodynamically. Diffusive mass exchange across the new interface, i.e., finger, perturbs the local interface leading to ramified fingers. Fractal-like fingering due to recursive diffusive-hydrodynamic mass exchange is self-sustained until equilibrium is achieved between the solvent and the crude-oil phases. (d) Slow diffusion of heavy crude oil-components with the light solvent phase results in a diffusive mixing zone ($t_{stageII}$). (For interpretation of the references to color in this figure legend, the reader is referred to the web version of this article.)

5. Conclusion

The two-stage spontaneous dispersive mechanism observed reveals a surprising mechanism that underlies the Saffman-Taylor instability for miscible, multicomponent fluids. In this work, mixing between heptane and a multicomponent crude oil were studied under no imposed advection (i.e., imposed Peclet number $Pe = 0$). Fractal-like fingers of solvent formed spontaneously. The fingers originated at the edge of the crude oil/heptane boundary and extended into the crude oil droplet without external pressure gradients. The direction of finger propagation was orthogonal to the original interface between the crude oil-solvent fluid-pair. Stage I of the two-stage interaction corresponded to rapid mass exchange between light components in the crude oil and the heptane. Interestingly, the rate of light component liberation, i.e., interface retraction velocity, was much larger than the diffusivity of heavy components into the heptane, and as a result a distinct dynamic interface was observed. Dynamic interfacial tension calculations based on the measured length and velocity quantities indicate a strong spatial gradient in dynamic interfacial tension. Fluid systems with gradients in interfacial tension experience diffusocapillary flow where convection cells are induced. The convection cells enhance light components extraction from the crude oil and thus propagate the spontaneous fingers. After light components erosion, heptane and the heavy components of the crude oil enter a purely diffusive regime, corresponding to stage II. The broader implications of this work are far-reaching and the physics discovered here provide a direct path to influence the energy industry. The hydrocarbon energy industry needs to remove as much carbon as possible from its production methods. Solvents, as studied in our paper, provide a means to produce viscous oils with dramatically reduced heat requirements. Importantly, the enhanced mixing of complex crude oils with solvents under micro/nanoconfinement discovered in this work opens up an opportunity for hydrocarbon recovery from shale. This work provides a bridge between physics and engineering as well as between current practice for EOR and future recovery technologies.

Acknowledgment

This work is supported by the SURPI-A Industrial Affiliates. W. Song gratefully acknowledges the financial support of the Gerald J. Lieberman Fellowship and the Hormoz and Fariba Ameri Graduate Fellowship.

References

[1] R.F. Meyer, E.D. Attanasi, P.A. Freeman, Heavy Oil and Natural Bitumen Resources in Geological Basins of the World, U.S. Geological Survey, 2007, p. 36.
[2] R.G. Santos, W. Loh, A.C. Bannwart, O.V. Trevisan, An overview of heavy oil properties and its recovery and transportation methods, Braz. J. Chem. Eng. 31 (3) (2014) 571–590, https://doi.org/10.1590/0104-6632.20140313s00001853.
[3] G. Hirasaki, D.L. Zhang, Surface chemistry of oil recovery from fractured, oil-wet, carbonate formations, SPE J. 9 (02) (2004) 151–162, https://doi.org/10.2118/88365-PA.
[4] A.R. Kovscek, Emerging challenges and potential futures for thermally enhanced oil recovery, J. Pet. Sci. Eng. 98–99 (2012) 130–143, https://doi.org/10.1016/j.petrol.2012.08.004.
[5] T.W. de Haas, H. Fadaei, U. Guerrero, D. Sinton, Steam-on-a-chip for oil recovery: the role of alkaline additives in steam assisted gravity drainage, Lab. Chip 13 (19) (2013) 3832–3839, https://doi.org/10.1039/c3lc50612f http://www.ncbi.nlm.nih.gov/pubmed/23835782.
[6] T. Boone, K. Sampath, D. Courtnage, Assessment of GHG emissions associated with in-situ heavy oil recovery processes, World Heavy Oil Congress, Aberdeen, Scotland, 2012.
[7] Z. Qi, A. Abedini, P. Lele, N. Mosavat, A. Guerrero, D. Sinton, Pore-scale analysis of condensing solvent bitumen extraction, Fuel 193 (2017) 284–293, https://doi.org/10.1016/j.fuel.2016.12.070 http://linkinghub.elsevier.com/retrieve/pii/S0016236116313011.
[8] T. Jiang, F. Zeng, X. Jia, Y. Gu, A new solvent-based enhanced heavy oil recovery

method: cyclic production with continuous solvent injection, Fuel 115 (2014) 426–433, https://doi.org/10.1016/j.fuel.2013.07.043.
[9] I. Bogdanov, S. Cambon, M. Mujica, A. Brisset, Heavy oil recovery via combination of radio-frequency heating with solvent injection, SPE Canada Heavy Oil Technical Conference (2016) 1–14, https://doi.org/10.2118/180709-MS.
[10] H. Li, S. Zheng, D. Yang, Enhanced Swelling Effect and Viscosity Reduction of Solvent(s)/CO2/Heavy-Oil Systems, Society of Petroleum Engineers, 2013, pp. 12–14, https://doi.org/10.2118/150168-pa (August).
[11] A. Prakoso, A. Punase, B. Hascakir, A Mechanistic Understanding of Asphaltene Precipitation From Varying Saturate Concentration Perspective, Society of Petroleum Engineers, 2015, https://doi.org/10.2118/177280-PA.
[12] W. Song, F. Ogunbanwo, M. Steinsbo, M. Ferno, A.R. Kovscek, Mechanisms of multiphase reactive flow using biogenically calcite-functionalized micromodels, Lab. Chip 577 (2018) 158–166.
[13] W. Song, A.R. Kovscek, Spontaneous clay pickering emulsification, Colloids Surf. A Physicochem. Eng. Asp. 577 (2019) 158–166.
[14] W. Song, T.W. de Haas, H. Fadaei, D. Sinton, Chip-off-the-old-rock: the study of reservoir-relevant geological processes with real-rock micromodels, Lab. Chip 14 (22) (2014) 4382–4390, https://doi.org/10.1039/C4LC00608A.
[15] L. Xu, A. Abedini, Z.B. Qi, M. Kim, A. Guerrero, D. Sinton, Pore-scale analysis of steam-solvent coinjection: azeotropic temperature, dilution and asphaltene deposition, Fuel 220 (November 2017) (2018) 151–158, https://doi.org/10.1016/j.fuel.2018.01.119.
[16] Z. Qi, A. Abedini, A. Sharbatian, Y. Pang, A. Guerrero, D. Sinton, Asphaltene deposition during bitumen extraction with natural gas condensate and naphtha, Energy Fuels (2017), https://doi.org/10.1021/acs.energyfuels.7b03495.
[17] W. Song, A.R. Kovscek, Functionalization of micromodels with kaolinite for investigation of low salinity oil-recovery processes, Lab. Chip 15 (2015) 3314–3325, https://doi.org/10.1039/C5LC00544B.
[18] W. Song, A.R. Kovscek, Direct visualization of pore-scale fines migration and formation damage during low-salinity waterflooding, J. Nat. Gas Sci. Eng. 34 (2016) 1276–1283, https://doi.org/10.1016/j.jngse.2016.07.055.
[19] A. Sell, H. Fadaei, M. Kim, D. Sinton, Measurement of CO2 diffusivity for carbon sequestration: a microfluidic approach for reservoir-specific analysis, Environ. Sci. Technol. 47 (1) (2013) 71–78.
[20] W. Song, H. Fadaei, D. Sinton, Determination of dew point conditions for CO2 with impurities using microfluidics, Environ. Sci. Technol. 48 (2014) 3567–3574.
[21] P.G. Saffman, S.G. Taylor, The penetration of a fluid into a porous medium or Hele-Shaw cell containing a more viscous liquid, Proc. R. Soc. A (1958).
[22] R.L. Chuoke, P. van Meurs, C. van der Poel, The instability of slow, immiscible, viscous liquid–liquid displacements in permeable media, Pet. Trans. AIME 216 (1959) 188–194 DOI: SPE-1141-G.
[23] G. Daccord, J. Nittmann, H.E. Stanley, Radial viscous fingers and diffusion-limited aggregation: fractal dimension and growth sites, Phys. Rev. Lett. 56 (4) (1986), https://doi.org/10.1103/PhysRevLett.56.336.
[24] G. Homsy, Viscous fingering in porous media, Annu. Rev. Fluid Mech. 19 (1987) 271–311.
[25] D.A. Weitz, J.P. Stokes, R.C. Ball, A.P. Kushnick, Dynamic capillary pressure in porous media: origin of the viscous-fingering length scale, Phys. Rev. Lett. 59 (26) (1987) 2967–2970, https://doi.org/10.1103/PhysRevLett.59.2967.
[26] Z. Yang, Y.C. Yortsos, Asymptotic solutions of miscible displacements in geometries of large aspect ratio, Phys. Fluids 9 (2) (1997) 286–298, https://doi.org/10.1063/1.869149.
[27] E. Lajeunesse, J. Martin, N. Rakotomalala, D. Salin, Y.C. Yortsos, Miscible displacement in a hele-shaw cell at high rates, J. Fluid Mech. 398 (1999) 299–319.
[28] N. Goyal, E. Meiburg, Miscible displacements in hele-shaw cells: two-dimensional base states and their linear stability, J. Fluid Mech. 558 (2006) 329–355, https://doi.org/10.1017/S0022112006009992.
[29] B. Jha, L. Cueto-Felgueroso, R. Juanes, Fluid mixing from viscous fingering, Phys. Rev. Lett. 106 (19) (2011) 194502, https://doi.org/10.1103/PhysRevLett.106.194502.
[30] I. Bischofberger, R. Ramachandran, S.R. Nagel, Fingering versus stability in the limit of zero interfacial tension, Nat. Commun. 5 (2014) 1–6, https://doi.org/10.1038/ncomms6265.
[31] X. Fu, L. Cueto-Felgueroso, R. Juanes, Viscous fingering with partially miscible fluids, Phys. Rev. Fluids 2 (10) (2017) 20–24, https://doi.org/10.1103/PhysRevFluids.2.104001.
[32] T.E. Videbæk, S.R. Nagel, Transition to Diffusion-Driven Viscous Fingering, (2018) arxiv:1803.07597.
[33] E. Lajeunesse, J. Martin, N. Rakotomalala, D. Salin, 3D instability of miscible displacements in a hele-shaw cell, Phys. Rev. Lett. 79 (26) (1997) 5254–5257, https://doi.org/10.1103/PhysRevLett.79.5254.
[34] P. Trevelyan, C. Almarcha, A. De Wit, Buoyancy-driven instabilities of miscible two-layer stratifications in porous media and Hele-Shaw cells, J. Fluid Mech. 670 (2011) 38–65.
[35] S. Pramanik, A. De Wit, M. Mishra, Viscous fingering and deformation of a miscible circular blob in a rectilinear displacement in porous media, J. Fluid Mech. 782 (2015).
[36] D. Truzzolillo, S. Mora, C. Dupas, L. Cipelletti, Off-equilibrium surface tension in colloidal suspensions, Phys. Rev. Lett. 112 (12) (2014).
[37] D. Truzzolillo, S. Mora, C. Dupas, L. Cipelletti, Nonequilibrium interfacial tension in simple and complex fluids, Phys. Rev. X 6 (4) (2016).
[38] D. Truzzolillo, L. Cipelletti, Off-equilibrium surface tension in miscible fluids, Soft Matter 13 (2017) 13–21.
[39] D. Truzzolillo, L. Cipelletti, Hydrodynamic instabilities in miscible fluids, J. Phys. Condens. Matter 30 (2018).
[40] T.W. Kim, E. Vittoratos, A.R. Kovscek, An experimental investigation of viscous-oil recovery efficiency as a function of voidage-replacement ratio, SPE J. 21 (04) (2016) 1236–1253, https://doi.org/10.2118/174032-PA.
[41] U.E. Guerrero-Aconcha, The Diffusion Coefficient of Liquid and Gaseous Solvents in Heavy Oil and Bitumen, Ph.D. Thesis, University of Calgary, 2009.
[42] J.W. Moore, R.M. Wellek, Diffusion coefficients of n-heptane and n-decane in n-alkanes and n-alcohols at several temperatures, J. Chem. Eng. Data 19 (2) (1974) 136–140, https://doi.org/10.1021/je60061a023.
[43] S. Lam, Multicomponent diffusion revisited, Phys. Fluids 18 (2006).
[44] J. Nittmann, G. Daccord, H.E. Stanley, Fractal growth viscous fingers: quantitative characterization of a fluid instability phenomenon, Nature (314) (1985) 141–144.
[45] P. Meakin, Diffusion-controlled cluster formation in 2-6 dimensional space, Phys. Rev. A 27 (3) (1983) 1495–1507, https://doi.org/10.1103/PhysRevA.27.1495 http://pra.aps.org/abstract/PRA/v27/i3/p1495_1.
[46] T.A. Witten Jr., L.M. Sander, Diffusion-limited aggregation, a kinetic critical phenomenon, Phys. Rev. Lett. 47 (1981).
[47] T.A. Witten Jr., L.M. Sander, Diffusion-limited aggregation, Phys. Rev. B 27 (1983).
[48] L. Paterson, Radial fingering in a Hele Shaw cell, J. Fluid Mech. 113 (1981) 513–529.
[49] M. Sahimi, Y.C. Yortsos, Pattern formation in viscous fingering: a diffusion-limited aggregation approach, Phys. Rev. A 32 (6) (1985) 3762–3764.
[50] O. Praud, H.L. Swinney, Fractal dimension and unscreened angles measured for radial viscous fingering, Phys. Rev. E – Stat. Nonlinear Soft Matter Phys. 72 (1) (2005) 1–10, https://doi.org/10.1103/PhysRevE.72.011406.
[51] W. Hayduk, B.S. Minhas, Correlations for prediction of molecular diffusivities in liquids, Can. J. Chem. Eng. 60 (1982) 295–299, https://doi.org/10.1002/cjce.5450600213.